

# Gravity waves from relativistic binaries

Janna Levin<sup>\*†</sup>, Rachel O'Reilly<sup>\*\*</sup> and E. J. Copeland<sup>\*\*</sup>

<sup>\*</sup>*Astronomy Centre, University of Sussex, Brighton BN1 9QJ, UK*

<sup>†</sup>*DAMTP, Cambridge University, Silver St., Cambridge CB3 9EW*

<sup>\*\*</sup>*Centre for Theoretical Physics, University of Sussex, Brighton BN1 9QJ, UK*

The stability of binary orbits can significantly shape the gravity wave signal which future Earth-based interferometers hope to detect. The inner most stable circular orbit has been of interest as it marks the transition from the late inspiral to final plunge. We consider purely relativistic orbits beyond the circular assumption. Homoclinic orbits are of particular importance to the question of stability as they lie on the boundary between dynamical stability and instability. We identify these, estimate their rate of energy loss to gravity waves, and compute their gravitational waveforms.

04.30.Db,97.60.Lf,97.60.Jd,95.30.Sf,04.70.Bw

Coalescing compact objects are proficient emitters of gravity waves during the final minutes before their demise. They are the most popular candidate for the direct detection of gravitational radiation by the future LIGO/VIRGO interferometers [1]. The gravitational wave frequencies sweep through the LIGO/VIRGO bandwidth of  $1 - 10^4$  Hz as the inspiral gives way to the plunge and final coalescence. General interest in the onset of the instability to a plunge has focused attention on the innermost stable circular orbit (ISCO) [2]. The post-Newtonian (PN) approximation to general relativity [3] has been studied in detail and the ISCO determined in the absence of dissipation in Ref. [4].

There are other orbits which may be even more important to the question of dynamical stability than the ISCO. The homoclinic orbit in particular arises at the boundary of the stable and unstable manifolds in the dynamics. A homoclinic orbit begins and ends asymptotically close to an unstable circular orbit, spiraling in and out around the center of mass. These trajectories define the region where dynamical instability, and even chaos, can develop [5]. Only black holes are compact enough to capture a companion in an orbit which approaches these smallest radii. We give a prescription for identifying homoclinic orbits in the 2PN expansion in the absence of dissipation, estimate the luminosity in gravity waves, and compute the gravitational waveform.

Long lived binaries will likely circularize by the time of inspiral as angular momentum is lost to gravity waves. In dense stellar regions such as globular clusters the capture of a companion can be an efficient mechanism for forming binaries [6]. There will not be sufficient time for these to circularize and we will have to accept them and their eccentricities. Recently some attention has been paid to gravity waves from more general orbits [7]. We use these advances to estimate the luminosity in gravity waves from a purely relativistic homoclinic orbit. In order to detect the waves, very precise theoretical templates are needed. The raw data will then be compared to the template over many thousands of orbits to draw out a detection. To keep the data analysis computationally manageable, the theoretical templates are primarily

for circular orbits. The homoclinic orbit will chirp up in frequency as it winds in toward the unstable circular orbit and then chirp down in frequency as it winds back out. To detect these, either more general templates, or new detection methods, are likely required.

## I. SCHWARZSCHILD BLACK HOLES

Primarily for a point of comparison, we estimate the rate of energy lost to gravitational waves and the waveforms for Schwarzschild black holes with a test mass companion in a relativistic orbit. In §II we find the energy loss and waveforms in the 2PN expansion. Schwarzschild geodesic motion is confined to an orbital plane and is described by the familiar metric

$$ds^2 = - \left(1 - \frac{2m}{R}\right) dt^2 + \left(1 - \frac{2m}{R}\right)^{-1} dR^2 + R^2 d\phi^2 \quad (1.1)$$

There are two constants of the motion; the energy  $E$  and the angular momentum  $J$  per unit rest mass:  $(1 - \frac{2m}{R}) t' = E + 1$  and  $R^2 \phi' = J$ , where a prime denotes differentiation with respect to an affine parameter. In order to compare with the 2PN approximation we have used the binding energy  $E$  which is equal to the usual Schwarzschild energy minus one. Working in Schwarzschild time  $t$ , the conserved angular momentum is

$$R^2 \dot{\phi} = \frac{J}{E + 1} \left(1 - \frac{2m}{R}\right) \quad (1.2)$$

and the energy constraint equation is

$$\frac{1}{2} \dot{R}^2 + V_{\text{eff}}(R) = 1 \quad (1.3)$$

with

$$V_{\text{eff}} \equiv 1 - \frac{1}{2} \left(1 - \frac{2m}{R}\right)^2 + \frac{1}{2(E+1)^2} \left(1 - \frac{2m}{R}\right)^3 \left(1 + \frac{J^2}{R^2}\right) \quad (1.4)$$

It is well known that for a large enough angular momentum, the black hole allows for two circular orbits; one unstable and one stable. The circular orbits are solutions to  $V_{\text{eff}} = 1$ . As was done in Ref. [5], the location, energy, and angular momentum of the circular orbits can be parameterized as

$$\begin{aligned} R_{un}/m &= \frac{6}{1+\beta} \\ R_{st}/m &= \frac{6}{1-\beta} \\ J/m &= 2\sqrt{\frac{3}{(1-\beta^2)}} \\ E_{un} &= -1 + \frac{(2-\beta)}{3}\sqrt{\frac{2}{(1-\beta)}} \\ m\dot{\phi}_{un} &= \frac{\sqrt{6}}{36}(1+\beta)^{3/2} . \end{aligned}$$

As the angular momentum and energy drop the two circular orbits move closer together and eventually meet at the ISCO. The ISCO is strictly speaking a saddle point of the dynamics and occurs for  $\beta = 0$  at  $R_{un} = R_{st} = 6$ ,  $m\dot{\phi} = \sqrt{6}/36$  and  $J/m = 2\sqrt{3}$ ,  $E = 2\sqrt{2}/3 - 1$ .

The ISCO is of interest as it marks the onset of a dynamical instability. There are other orbits which may be even more important to the question of the dynamical stability. The homoclinic orbits are defined as those trajectories which asymptotically approach the same unstable orbit in the infinite past as they do in the infinite future. These orbits lie in the most unstable region of phase space and will be the site of any chaotic dynamics which may develop as a result of perturbations [5]. In the binary system they begin infinitesimally close to an unstable circular orbit, wind out to a maximum radius and then wind back in again just reaching the unstable orbit.

A trajectory which begins high on an unstable circular orbit has enough energy to escape the pair if its energy exceeds the asymptotic energy of a companion at rest at infinity; that is if  $E > 0$ . The homoclinic orbit can therefore only exist if  $E < 0$  at the unstable circular orbit. The first homoclinic orbit appears when  $\beta = 1/2$  and asymptotically reaches the unstable circular orbit at  $R_*/m = 4$ ,  $m\dot{\phi}_* = 1/8$  and  $J_*/m = 4$ . Bombelli and Calzetta [5] found the homoclinic orbit explicitly as

$$\frac{m}{R} = \frac{(1-2\beta)}{6} + \beta \tanh^2\left(\sqrt{\beta}\phi/2\right). \quad (1.5)$$

with the range  $0 < \beta < 1/2$ .

No pair will ever reside exactly at the homoclinic orbit. More naturally, we show a nearly homoclinic orbit obtained by starting a pair at the homoclinic  $J/m$  for  $\beta = 0.47$  but with a radius  $0.01m$  larger than the unstable circular orbit. The trajectory is shown in fig. 1. The companion executes a few windings around the unstable circular orbit before tracing the giant precessing

ellipse. This path is much more interesting than a simple Keplerian elliptical orbit as is the gravitational waveform generated.

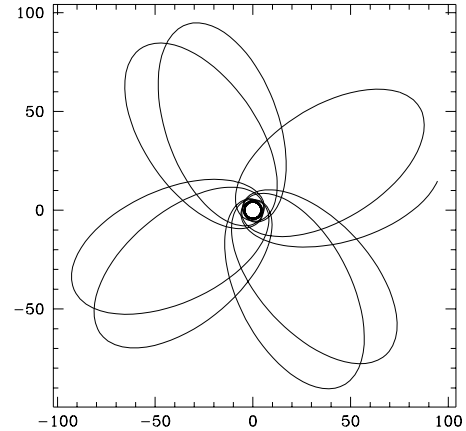


FIG. 1.  $\beta = .47$ ,  $R = R_{un} + 0.01$ ,  $\dot{r} = 0$

We calculate the luminosity in gravity waves and the waveform for the homoclinic orbits in the Newtonian quadrupole approximation. Strictly speaking, the Newtonian approximation is not appropriate for use with gravitational sources. In §II, we utilize the waveforms properly estimated in the 2PN expansion of the two-body problem. The qualitative behaviour is strikingly similar to the quadrupole approximation of this section. The Schwarzschild solution may also have a role in the computation of the two-body expansion. In the test mass limit, the 2PN expansion converges slowly to the Schwarzschild solution. For this reason a hybrid expansion of the equations of motion has been proposed which is exactly Schwarzschild in the test mass limit [4]. A similar hybrid expansion of the waveforms could reduce to these Schwarzschild expressions for a massive black hole with a light companion.

The quadrupole moment is simply  $I_{ij} = mx_ix_j$ :

$$\begin{aligned} I_{xx} &= mR^2 \cos^2 \phi \\ I_{yy} &= mR^2 \sin^2 \phi \\ I_{xy} &= mR^2 \cos \phi \sin \phi \end{aligned}$$

with all other components zero. The luminosity in gravity waves is estimated as

$$L_{GW} = \frac{1}{5} \left\langle \ddot{F}_{xx}^2 + \ddot{F}_{yy}^2 + \ddot{F}_{zz}^2 + 2\ddot{F}_{xy}^2 \right\rangle \quad (1.6)$$

with the notation

$$F_{ij} = I_{ij} - \frac{1}{3}\delta_{ij}I_k^k. \quad (1.7)$$

For a general orbit, this can be expressed as

$$L_{GW} = \frac{1}{5} \frac{m^2}{2} \langle Q^2 + P^2 + 3W^2 \rangle \quad (1.8)$$

with

$$W = \frac{2}{3}(\dot{R} \ddot{R} + 3\dot{R}\ddot{R}) \quad (1.9)$$

$$Q = 2\dot{R} \ddot{R} + 6\dot{R}\ddot{R} - 24\dot{R}\dot{\phi}^2 - 12R^2\dot{\phi}\ddot{\phi} \quad (1.10)$$

$$P = 12\dot{R}\ddot{R}\dot{\phi} + 12\dot{R}^2\dot{\phi} + 12\dot{R}\ddot{R}\ddot{\phi} + 2R^2\dot{\phi}\ddot{\phi} - 8R^2\dot{\phi}^3 \quad (1.11)$$

The instantaneous rate of energy loss to gravity waves is shown in the top panel of fig. 2. As expected, the luminosity is greatest when the binary is closest together although the pair spends a longer time at larger separations. For  $\beta = 0$ , the homoclinic orbit and the unstable circular orbit are one and the same and the luminosity reduces to the expected circular orbit expression. For the exact homoclinic orbit the solution eqn. (1.5) can be substituted into eqn. (1.8) to write the luminosity as a function of  $\phi$  only. However, the expression is long and involved and not particularly illuminating. We present the numerical results instead.

The transverse, traceless waveform can be estimated using the Newtonian quadrupole

$$h_{ij}^{TT} = \frac{2}{D}\ddot{I}_{ij}^{TT} \quad (1.12)$$

with the Earth a distance  $D$  from the pair in a direction  $\hat{N}$ ,  $\ddot{I}_{ij}^{TT} = P_{ijkl}\ddot{I}_{km}$ , and

$$P_{ijkl} = (\delta_{ik} - N_i N_k)(\delta_{jm} - N_j N_m) - \frac{1}{2}(\delta_{ij} - N_i N_j)(\delta_{km} - N_k N_m). \quad (1.13)$$

For the sake of illustration we place the Earth directly above the binary so that  $\hat{N} = \hat{z}$ . The waveforms for the two polarizations are  $h_+ = h_{xx} = -h_{yy}$

$$h_+ = \frac{1}{D}(\ddot{I}_{xx} - \ddot{I}_{yy}) \quad (1.14)$$

$$= \frac{2m}{D}((\dot{R}^2 + R\ddot{R} - 2R^2\dot{\phi}^2)\cos 2\phi - (4R\dot{R}\dot{\phi} + R^2\ddot{\phi})\sin 2\phi)$$

and

$$h_\times = h_{xy} = h_{yx} = \frac{2}{D}\ddot{I}_{xy} \quad (1.15)$$

$$= \frac{2m}{D}((\dot{R}^2 + R\ddot{R} - 2R^2\dot{\phi}^2)\sin 2\phi + (4R\dot{R}\dot{\phi} + R^2\ddot{\phi})\cos 2\phi).$$

The observer can be moved without complication to an arbitrary location by using rotated quadrupole components,  $\bar{I} = O^T I O$  with  $O(\hat{N})$  the appropriate rotation matrix. A detector will respond to a linear superposition of  $h_+$  and  $h_\times$ . The bottom panel of fig. 2 is the waveform  $h_+$  for the orbit of fig. 1. The middle panel focuses in on a shorter time interval to resolve the oscillations as the companion sweeps near the unstable circular orbit. This signal appears to chirp periodically. Although we have only used the Newtonian approximation, we will show in the next section that the 2PN estimation of the two body problem mimics these features with little alteration.

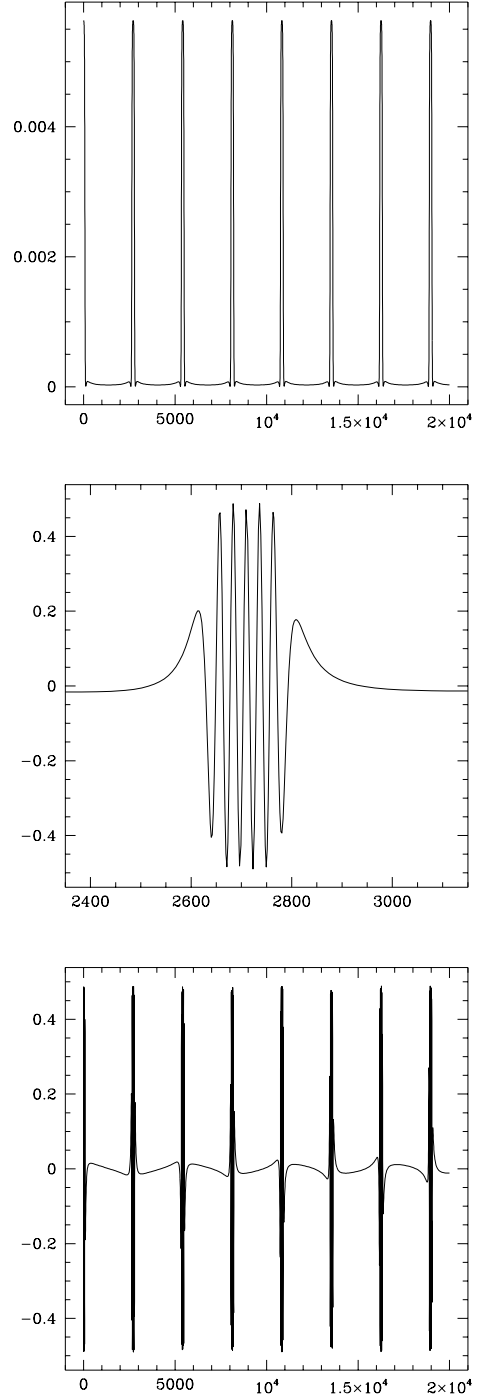


FIG. 2. Top: The luminosity in gravity waves for the orbit of fig. 1 as a function of  $t/m$ . Middle: The waveform  $h_+$  over a short interval. Bottom: The waveform  $h_+$  over a longer interval. The scale of  $h_+$  is arbitrary.

We show another nearly homoclinic orbit in fig. 3 for  $\beta = 0.3$  which has the angular momentum of the unstable circular orbit but begins displaced by  $0.01m$  from the circular radius. This orbit again winds tightly around the unstable circular orbit before tracing a wider orbit. The rate of energy loss to gravitational waves is shown in

the middle panel of fig. 3 and the waveform  $h_+$  is shown in the bottom panel.

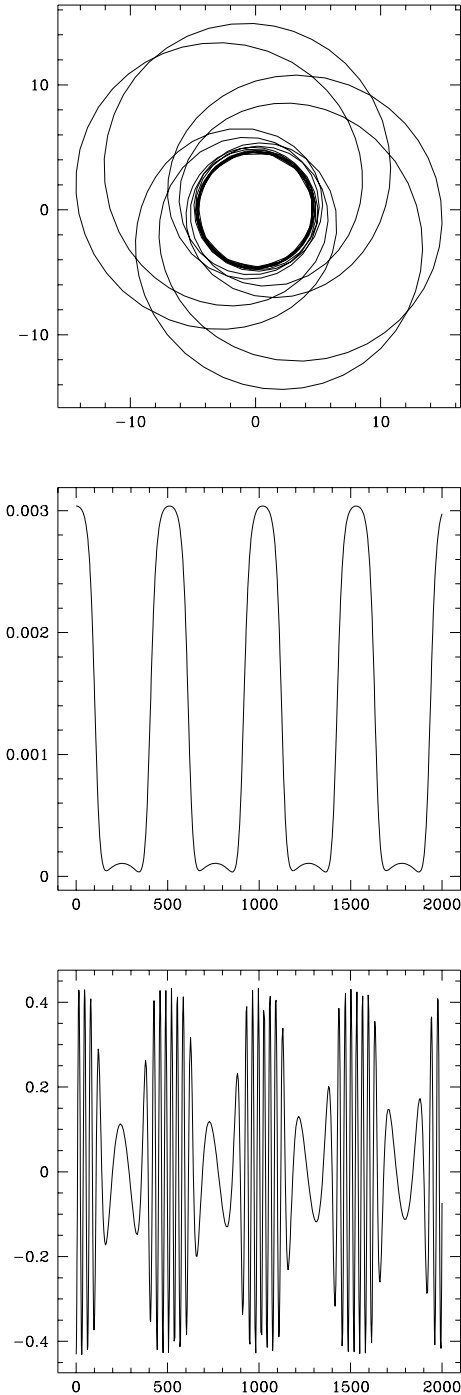


FIG. 3. The orbit, waveform and the rate of energy loss for a nearly homoclinic orbit with  $\beta = .3$ ,  $R = R_{un} + 0.01$ ,  $\dot{R} = 0$ .

This can be compared to the waveform for an elliptical orbit calculated in the Newtonian approximation [8,9]. The elliptic orbits have similar peaks and drops but do not have the multiple oscillations inbetween.

## II. THE 2PN EXPANSION

The Schwarzschild solutions of the previous section can be compared to the post-Newtonian approximations of the two-body problem. In the 2PN expansion, the center of mass equations of motion for the binary orbit can be written in harmonic coordinates as [4,10,11]

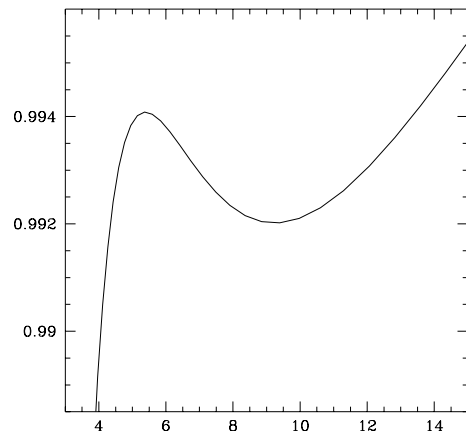
$$\ddot{r} = r\dot{\phi}^2 - \frac{m}{r^2} (A + B\dot{r}) \quad (2.1)$$

$$\ddot{\phi} = -\dot{\phi} \left( \frac{m}{r^2} B + 2\frac{\dot{r}}{r} \right) \quad (2.2)$$

where  $m = m_1 + m_2$  is the total mass of the pair and for future use we define the product of reduced masses  $\eta = m_1 m_2 / m^2$ . In the test mass limit,  $\eta = 0$ , the harmonic coordinates are related to the familiar Schwarzschild coordinates by  $r = R - m$ . The form of  $A(r, \dot{r}, \dot{\phi})$  and  $B(r, \dot{r}, \dot{\phi})$  depends on the order of the PN expansion and can be found in the Appendix. To 2PN order there are two constants of motion, the energy  $E(r, \dot{r}, \dot{\phi})$  and the angular momentum  $J(r, \dot{r}, \dot{\phi})$  per unit rest mass. These elaborate expressions are also recorded in the Appendix. The two constants of motion can be used in principle to eliminate  $\dot{r}$  and  $\dot{\phi}$  from eqn. (2.1). Just as with the Schwarzschild solution, the orbital dynamics can be reduced to the study of one-dimensional motion in an effective potential,  $\ddot{r} = -\partial V_{\text{eff}}(r) / \partial r$ . Integrating we have

$$\frac{1}{2} \dot{r}^2 + V_{\text{eff}}(r) = \text{constant}. \quad (2.3)$$

The constant is arbitrary and we shall hereafter set it to 1. We will use eqn. (2.3) as a definition of  $V_{\text{eff}}$  in the numerical solutions. A typical  $V_{\text{eff}}$  for a black hole binary is shown in fig. 4, obtained by throwing the pair together at 2PN order and integrating to find  $V_{\text{eff}} = 1 - (1/2)\dot{r}^2$ . The shape of the potential does depend on both  $E$  and  $J/m$  but nonetheless this typical  $V_{\text{eff}}$  gives an indication of the location of two circular orbits: one unstable circular orbit near the maximum and one stable circular orbit near the minimum.



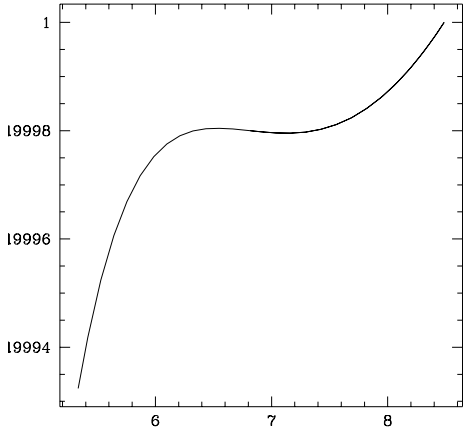


FIG. 4. The 2PN  $V_{\text{eff}} = 1 - (1/2)\dot{r}^2$  with  $\eta = 1/4$  for two trajectories. Top: Initial conditions are  $r/m = 20$ ,  $\dot{r} = -0.02$ ,  $m\dot{\phi} = 0.008$ . The potential depends on both the energy,  $E = -0.01298$ , and the angular momentum,  $J/m = 3.3067$ . Bottom: The initial conditions are  $r/m = 6.8172$ ,  $m\dot{\phi} = 0.05176$  which are ISCO values for  $\eta = 1/4$  but with  $\dot{r} = 0.02$  initially.

To find the homoclinic orbit, we first find all of the circular orbits. For circular motion,  $\ddot{r}_o = \dot{r}_o = 0$ . From eqn. (2.1) this demands [4]

$$\dot{\phi}_o^2 = \frac{mA_o}{r_o^3}. \quad (2.4)$$

We solve the circular orbit condition (2.4) for  $\dot{\phi}_o(r_o)$  as a function of the radius of the circular orbit and the ratio of masses  $\eta$ . The solution is provided in the Appendix eqn. (A6) for reference and provides the complete initial conditions for circular orbits. We substitute  $\dot{\phi}_o$  into  $J$  to define an angular momentum along circular orbits

$$\bullet \quad J_o(r_o) \equiv J(r_o, \dot{r}_o = 0, \dot{\phi}_o) \quad (2.5)$$

and into  $E$  to define an energy along circular orbits

$$\bullet \quad E_o(r_o) \equiv E(r_o, \dot{r}_o = 0, \dot{\phi}_o). \quad (2.6)$$

These are functions of  $r_o$  only, once  $\eta$  is specified. We find the smallest circular radius,  $r_*$ , for which

$$\bullet \quad E_o(r_*) < 0. \quad (2.7)$$

The first homoclinic orbit begins at this unstable circular orbit. As the angular momentum and the energy decrease, the last homoclinic orbit coincides with the ISCO. All homoclinic orbits can therefore be found by finding  $r_*$  and  $r_{\text{ISCO}}$  as functions of  $\eta$ .

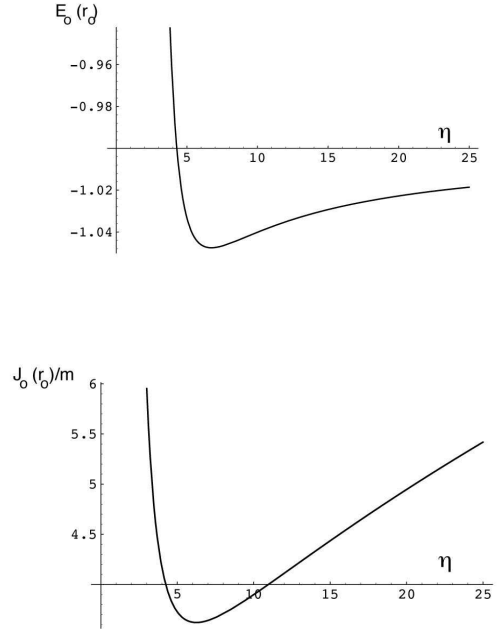
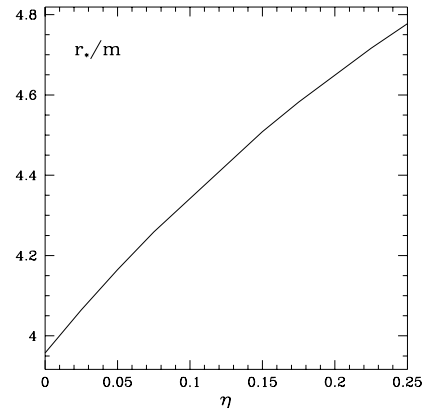


FIG. 5. The energy along circular orbits (top) and the angular momentum along circular orbits (bottom) in the 2PN expansion with  $\eta = 0.1/(1.1)^2$ .

For a companion of mass 1/10th its partner,  $\eta = 0.1/(1.1)^2$  then  $E_o(r_o)$  and  $J_o(r_o)/m$  are shown in fig. 5. For unstable circular orbits greater than  $r_*/m = 4.2866$ ,  $E < 0$ . This can be repeated for any  $\eta$  to generate figs. 6. These show the values of  $r_*/m$ , the orbital frequency  $f_* = \dot{\phi}/(2\pi)$ , and  $J_*/m$  for the unstable circular orbit when  $E_* = 0$  as functions of  $\eta$ .



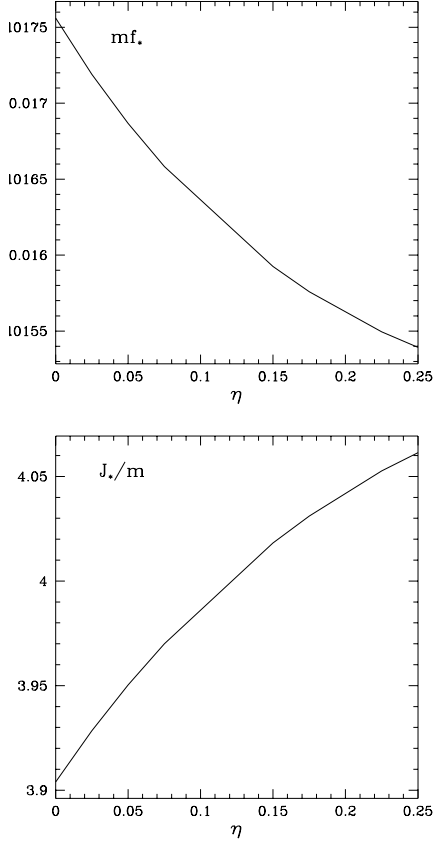


FIG. 6. The radius (top), the orbital frequency (middle), and angular momentum (bottom) of the smallest unstable circular orbit for which there is a homoclinic orbit as functions of  $\eta$  in the 2PN expansion. The energy by definition is zero.

We follow Ref. [4] to locate the ISCO. The stability of the fixed points is tested by perturbing eqns. (2.1)-(2.2) about  $(r_o, \dot{r}_o = 0, \dot{\phi}_o)$  to obtain,

$$\frac{d}{dt} \begin{pmatrix} \delta r \\ \delta \dot{r} \\ \delta \dot{\phi} \end{pmatrix} = \begin{pmatrix} 0 & 1 & 0 \\ a & 0 & b \\ 0 & c & 0 \end{pmatrix} \begin{pmatrix} \delta r \\ \delta \dot{r} \\ \delta \dot{\phi} \end{pmatrix} \quad (2.8)$$

where

$$\begin{aligned} a &= 3\dot{\phi}_o^2 - \frac{m}{r_o^2} \left( \frac{\partial A}{\partial r} \right)_o \\ b &= 2r_o \dot{\phi}_o - \frac{m}{r_o^2} \left( \frac{\partial A}{\partial \dot{\phi}} \right)_o \\ c &= -\dot{\phi}_o \left( \frac{2}{r_o} + \frac{m}{r_o^2} \left( \frac{\partial B}{\partial \dot{r}} \right)_o \right). \end{aligned} \quad (2.9)$$

The perturbations obey

$$\begin{pmatrix} \delta r \\ \delta \dot{r} \\ \delta \dot{\phi} \end{pmatrix} \propto e^{i\lambda t} \quad (2.10)$$

with  $i\lambda$  the eigenvalues of (2.8),

$$\lambda = 0, \quad \lambda = \pm(-a - bc)^{1/2}. \quad (2.11)$$

Stable oscillations about a circular orbit correspond to real  $\lambda$  so that  $a + bc < 0$ . The ISCO is the minimum value of  $r_o$  that has a real  $\lambda$  and satisfies condition (2.4) [4].

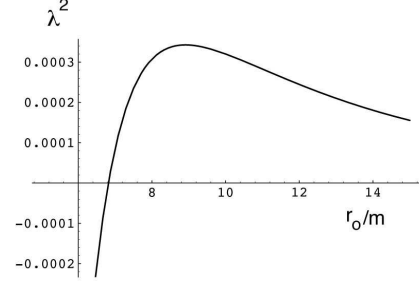


FIG. 7.  $\lambda^2$  along circular orbits in the 2PN expansion with  $\eta = 1/4$ .

Using eqn. (A1) for  $A$  and eqn. (A2) for  $B$ , we find  $\dot{\phi}_o(r_o)$  in eqn. (A6). The resultant  $\lambda^2(r_o)$  is illustrated in fig. (7) for an equal mass companion. For any  $\eta$ , the values of  $r_{\text{isco}}$ , the orbital frequency  $f_{\text{isco}} = \dot{\phi}/(2\pi)$ ,  $E_{\text{isco}}$  and  $J_{\text{isco}}$  are shown in figs. 8-9.

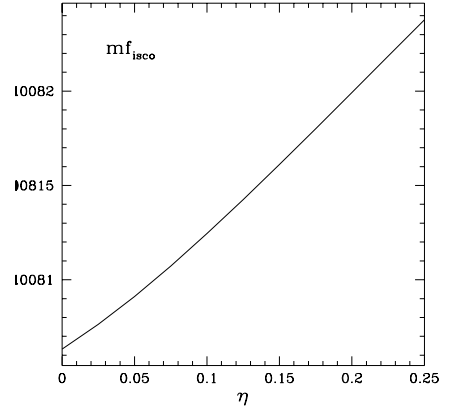
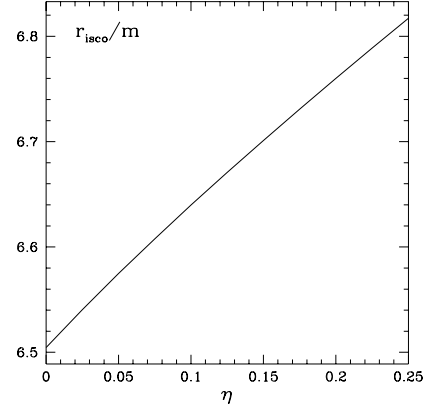


FIG. 8. The radius (top) and frequency (bottom) of the ISCO as functions of  $\eta$  in the 2PN expansion.

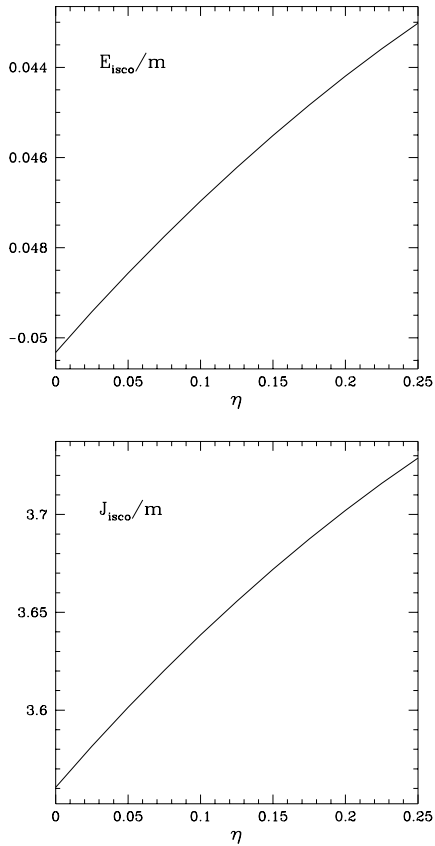


FIG. 9. The energy (top) and the angular momentum (bottom) of the ISCO as functions of  $\eta$  in the 2PN expansion.

With the ISCO and the critical unstable circular orbit we have the initial conditions for any homoclinic orbit in the 2PN expansion.

### A. Nearly homoclinic paths

An example of a nearly homoclinic orbit for  $\eta = 0.1/(1.1)^2$  is obtained numerically by starting on an unstable circular orbit at  $r/m = 4.409$  and knocking the orbit slightly outwards. The binary orbit is not just a simple precessing ellipse. The orbit first glides around the unstable circular orbit, then executes a giant ellipse, swings around the inner unstable circular orbit again before tracing another ellipse in a nearly opposite direction. This overall interleaved tracing then precesses. This orbit is relativistic and is not even *quasi*-Keplerian. Snapshots of the orbit are shown in fig. 10 and fig. 11 shows the effective potential. A phase space diagram shows periodicity in  $(r, \dot{r})$  in fig. 12.

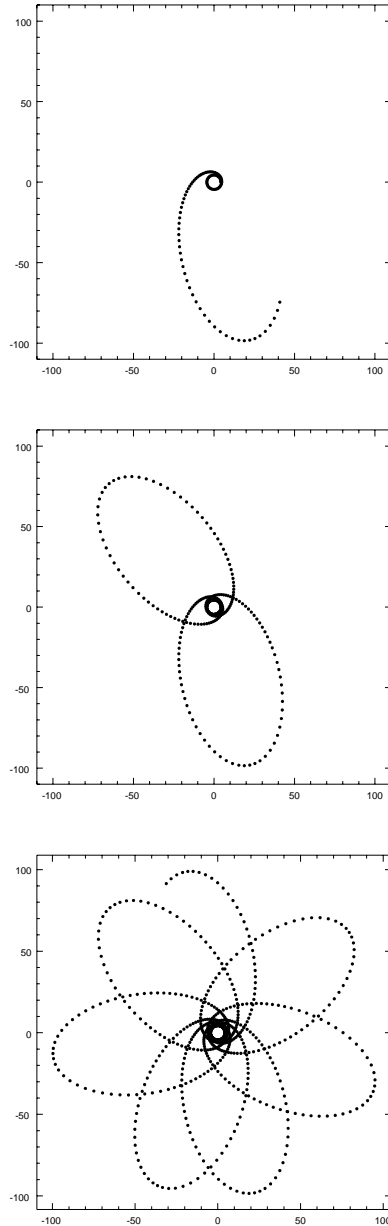


FIG. 10. A series of snap shots for a nearly homoclinic orbit. The ratio of masses is  $m_2/m_1 = 0.1$  so that  $\eta = 0.082644628$ . The initial conditions were  $r/m = 4.409$ ,  $\dot{r} = 0$ ,  $m\dot{\phi} = 0.0985406$ . Consequently  $E = -0.0084324135$  and  $J/m = 3.9166041778$ .

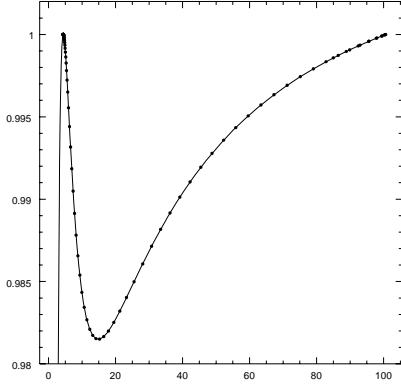


FIG. 11. The solid line is the full potential while the dots indicate that part of the potential traced out by the relativistic orbit.

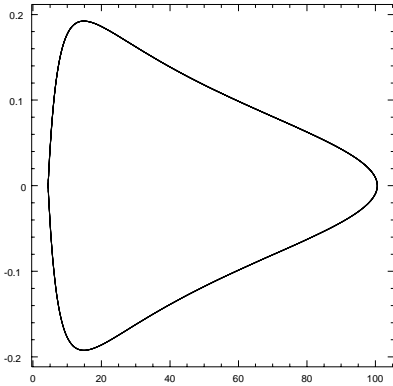


FIG. 12. The phase space  $(r, \dot{r})$  for the trajectory of fig. 10.

The gravitational wave frequency measured by a distant observer is roughly twice the orbital frequency for a circular orbit. For elliptical orbits the waves oscillate at once, twice and three times the orbital frequency [9]. Since the orbital frequency here is not constant, the comparison is more ambiguous. The waveform oscillates roughly twice per winding around the center of mass. The orbital frequency in units of  $Hz$  is

$$\left(\frac{m}{1.4M_{\odot}}\right) f = \frac{\dot{\phi}}{2\pi} \left(\frac{c^3}{1.4GM_{\odot}}\right) \text{ Hz}, \quad (2.12)$$

and is shown in fig. 13. For a pair with a total mass twice  $1.4M_{\odot}$ , the frequency  $\sim \mathcal{O}(2000)$  Hz at the circular orbit and drops to  $\mathcal{O}(10)$  Hz. Although these frequencies are still within the LIGO range, the signal will appear to chirp up and then down again. For black hole pairs with larger total mass, the signal will move in and out of LIGO's bandwidth.

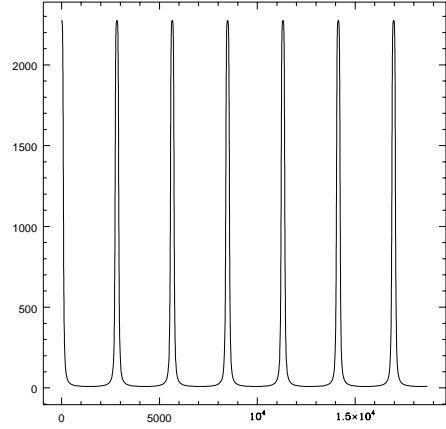
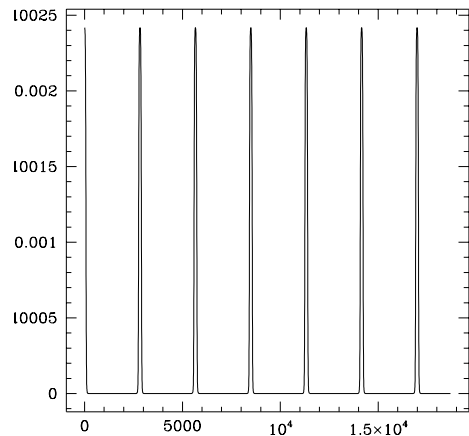


FIG. 13. The orbital frequency of eqn. (2.12) measured in Hz as a function of  $t/m$ .

It is unclear if a circular orbit template integrated against data which chirps in and out will lock onto a signal. The far-zone energy and angular momentum flux is calculated in Ref. [7] for general binary orbits in the 2PN formalism. We use their results (quoted in the Appendix) to draw  $L_{GW}$  in the top panel of fig. 14. As expected the rate of energy loss is greatest near the unstable circular orbit but the orbit spends much more time emitting gravity waves at the lower rate.

Also shown is the waveform along this orbit using the 2PN approximation to the far-zone waveform of Ref. [7]. We have written the results of Ref. [7] for  $h_{km}^{TT}$  in the Appendix eqn. (A13). Notice how strikingly similar the 2PN waveform is to the Newtonian approximation for the waveform from the similar Schwarzschild orbit of figs. 1 & 2.





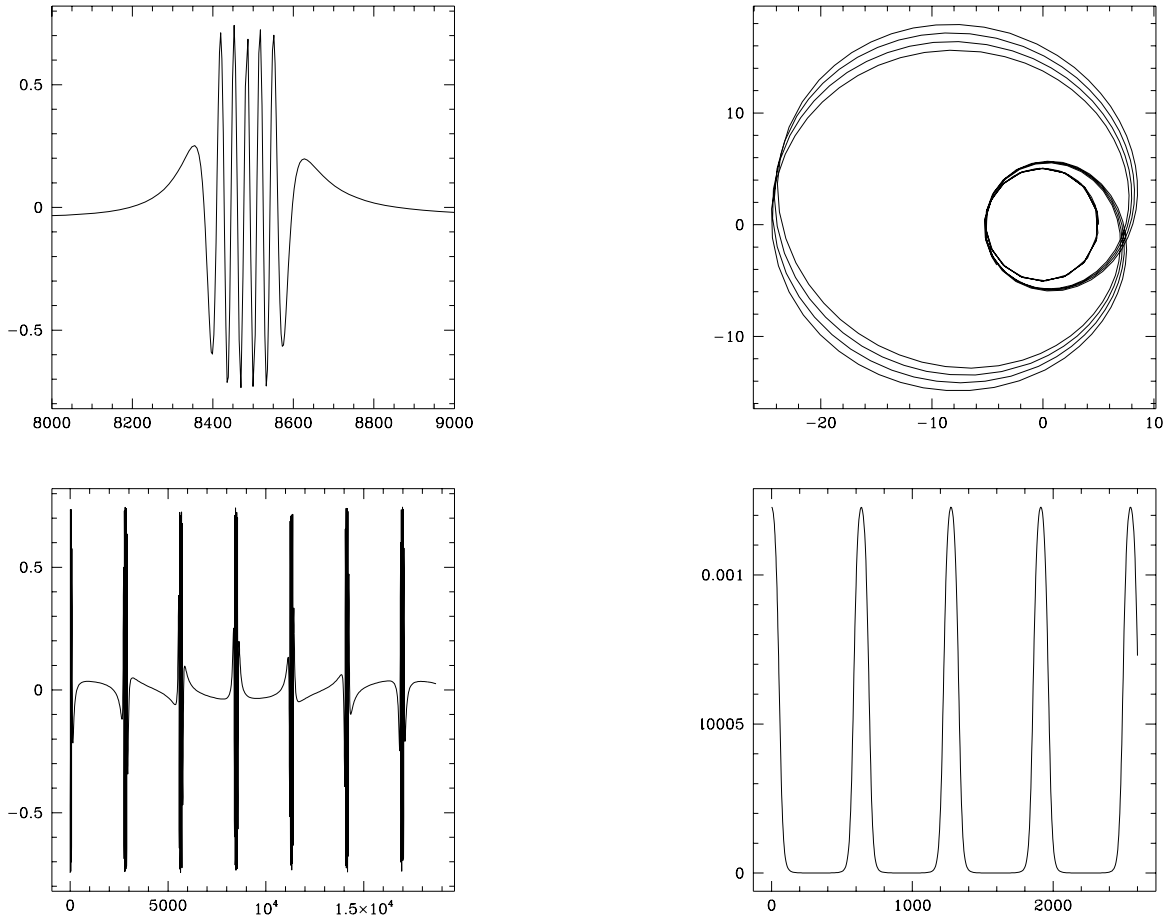


FIG. 14. Top: The rate of energy loss to gravitational waves for the orbit of fig. 10 as a function of  $t/m$ . Middle: Resolution of the waveform  $h_+$  for a short interval. Top: The waveform  $h_+$  over the entire interval of the orbit of fig. 10. The scale is arbitrary.

We find another nearly homoclinic orbit for equal mass binaries so that  $\eta = 1/4$ . We begin the orbit at

$$r_i/m = 5.01 \quad m\dot{\phi}_i = 0.0886. \quad (2.13)$$

These initial conditions are the same as the corresponding unstable circular orbit but with initial radius  $0.01m$  greater. The orbit, luminosity in gravity waves, and the waveform  $h_+$  are shown in fig. 15. Notice that the waveform  $h_+$  oscillates several times during the sweep around the unstable circular orbit. Again, there is a striking similarity between the 2PN waveforms and the waveforms calculated in the quadrupole approximation for the Schwarzschild orbit of fig. 3.

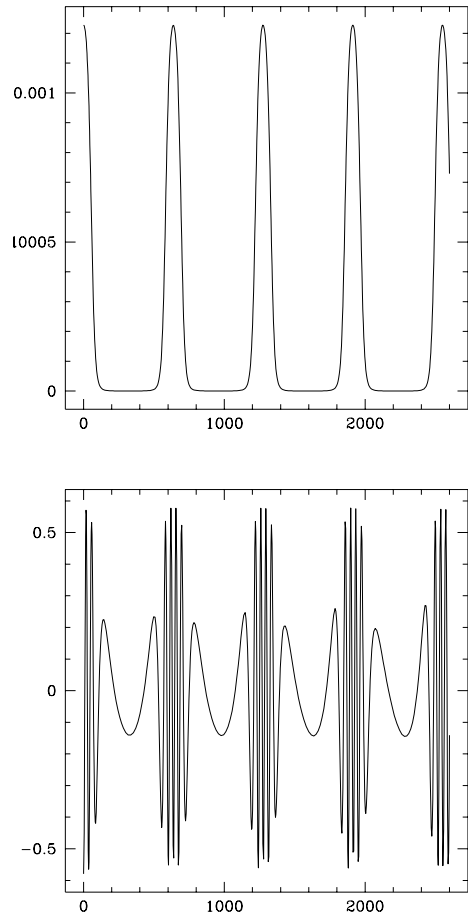


FIG. 15. Middle: Top: Another nearly homoclinic orbit with initial values as in eqn. (2.13). The rate of energy loss to gravitational waves for the above orbit. Bottom: The waveform  $h_+$ .

It is difficult to say how generic these relativistic orbits are in a realistic capture scenario. Clearly eccentric orbits are more likely than circular ones. For angular momenta in the range  $J_{\text{isco}} < J < J_o$ , these relativistic orbits are most natural. If a black hole captures a companion in an initially eccentric quasi-Keplerian orbit. The angular

momentum and energy lost to gravity waves will not be sufficient to circularize prior to plunge but may drive the pair into the range  $E < 0$  and  $J < J_o$  and therefore onto a winding relativistic orbit.

Although the frequencies are within the LIGO detection bandwidth, these waveforms may not be detectable by the method of matched filtering against circular templates. Eccentric signals matched against circular filters result in a loss in signal-to-noise [9]. The chirping up and down of these relativistic signal makes them even more difficult to pick up with a circular template. A quantitative analysis of the loss in signal-to-noise is currently underway.

The effect of the radiative back reaction on the instability is also important. Dissipation due to radiative back reaction appears at 5/2PN-order. The location of the circular orbits is unaffected by these terms. The circular orbits still obey eqn. (2.4) and  $A(r_o, \dot{r}_o = 0, \dot{\phi}_o)$  is the same with or without radiative back reaction since the 5/2PN contribution to  $A$  (eqn. (A8)) is proportional to  $\dot{r}$ . The stability of a given  $r_o$  will however be affected. Dissipation will likely make orbits more unstable and intuition would suggest the ISCO would move outward. A binary on a nearly homoclinic path may plunge together as a result of energy loss which pushes the pair beyond the unstable asymptote. Alternatively, they may fall into a decaying oscillation about the stable point, gradually spiraling together. Which outcome results will depend on the initial conditions of the specific orbit.

Even more intriguing is the possibility that the gravity waves disrupt the orbit to the point of chaos. A hypothetical gravitational wave can, under certain conditions, lead to a stochastic region along the homoclinic orbit [5]. The importance of this is clear. Chaos may be an inevitable element in both the coalescence and the gravity wave spectrum [12]. However, the strength, frequency, and waveform specific to the binary may not have the right form to induce chaos. With the waveforms for general orbits of Ref. [7] and the homoclinic orbits we have isolated, a more realistic search for chaos in coalescing binaries is possible.

## ACKNOWLEDGMENTS

We thank Bernard Schutz for insightful comments in the early stages of this work. We gratefully acknowledge PPARC support. EJC thanks the Isaac Newton Institute for hospitality.

- [2] N.Wex and G.Schäfer, *Class. Quant. Grav.* **10** 2729 (1993); J.R.Wilson and G.J.Mathews, *Phys. Rev. Lett.* **75** 4161 (1995); D.M Eardly and E.W. Hirschmann, gr-qc 9601019; D.Lai and A.G.Wiseman, *Phys. Rev. D.* **54** 3958 (1996).
- [3] See for instance T.Damour in *300 Years of Gravitation*, ed. S.W.Hawking and W.Israel (Cambridge University Press, Cambridge, England, 1987) p.128.
- [4] L.E.Kidder, C.M.Will and A.G.Wiseman, *Phys. Rev. D.* **47** 3281 (1993).
- [5] L.Bombelli and E.Calzetta, *Class. Quantum. Grav.* **9** 2573 (1992).
- [6] G.Quinlan and S.L.Shapiro, *Astrophys. J.* **321** 199 (1987).
- [7] A.Gopakumar and B.R.Iyer, *Phys. Rev. D.* **59** 7708 (1997).
- [8] H.Walquist, *Gen. Rel. Grav.* **19** 1101 (1987).
- [9] K.Martel and E.Poisson, gr-qc/9907006.
- [10] C.W.Lincoln and C.M.Will, *Phys. Rev. D.* **42** 1123 (1990).
- [11] T. Damour and N. Deruelle, *C. R. Acad. Sci. Paris* **293** 573 (1981); **293** 877 (1981).
- [12] J.Levin, *Phys. Rev. D.* **60** 64015 (1999).

---

[1] K.S.Thorne, gr-qc/9704042.

## APPENDIX A: 2PN EQUATIONS OF MOTION, LUMINOSITY AND WAVEFORMS

The center of mass equations of motion for the relativistic binary can be written as

$$\begin{aligned}\ddot{r} &= r\dot{\phi}^2 - \frac{m}{r^2}(A + B\dot{r}) \\ \ddot{\phi} &= -\dot{\phi}\left(\frac{m}{r^2}B + 2\frac{\dot{r}}{r}\right)\end{aligned}$$

[4,10,11]. The equations for  $A$ ,  $B$ ,  $E$  and  $J$  can be found in Ref. [4,10,11] and are included here for the purposes of keeping the paper self-contained. In the PN expansion, the expression for  $A$  and  $B$  can be obtained order by order in the small quantity  $v^2 = \dot{r}^2 + r^2\dot{\phi}^2$ . To 2PN order

$$A = 1 + A_1 + A_2 \tag{A1}$$

with

$$\begin{aligned}A_1 &= -2(2 + \eta)\frac{m}{r} + (1 + 3\eta)v^2 - \frac{3}{2}\eta\dot{r}^2 \\ A_2 &= \frac{3}{4}(12 + 29\eta)\left(\frac{m}{r}\right)^2 + \eta(3 - 4\eta)v^4 + \frac{15}{8}\eta(1 - 3\eta)\dot{r}^4 \\ &\quad - \frac{3}{2}\eta(3 - 4\eta)v^2\dot{r}^2 - \frac{1}{2}\eta(13 - 4\eta)\frac{m}{r}v^2 \\ &\quad - (2 + 25\eta + 2\eta^2)\frac{m}{r}\dot{r}^2\end{aligned}$$

and

$$B = B_1 + B_2 \tag{A2}$$

with

$$\begin{aligned}B_1 &= -2(2 - \eta)\dot{r} \\ B_2 &= -\frac{1}{2}\dot{r}\left[\eta(15 + 4\eta)v^2 - (4 + 41\eta + 8\eta^2)\frac{m}{r} - 3\eta(3 + 2\eta)\dot{r}^2\right]\end{aligned}$$

The subscripts refer to the order of the term in the PN expansion. To 2PN order, there is no dissipation yet included and there are two conserved quantities: The reduced energy and the reduced angular momentum,

$$\begin{aligned}E &= \frac{1}{2}v^2 - \frac{m}{r} + \frac{3}{8}(1 - 3\eta)v^4 + \frac{1}{2}(3 + \eta)v^2\frac{m}{r} + \frac{1}{2}\eta\frac{m}{r}\dot{r}^2 + \frac{1}{2}\left(\frac{m}{r}\right)^2 \\ &\quad + \frac{5}{16}(1 - 7\eta + 13\eta^2)v^6 + \frac{1}{8}(21 - 23\eta - 27\eta^2)\frac{m}{r}v^4 + \frac{1}{4}\eta(1 - 15\eta)\frac{m}{r}v^2\dot{r}^2 \\ &\quad - \frac{3}{8}\eta(1 - 3\eta)\frac{m}{r}\dot{r}^4 + \frac{1}{8}(14 - 55\eta + 4\eta^2)\left(\frac{m}{r}\right)^2v^2 + \frac{1}{8}(4 + 69\eta + 12\eta^2)\left(\frac{m}{r}\right)^2\dot{r}^2 - \\ &\quad - \frac{1}{4}(2 + 15\eta)\left(\frac{m}{r}\right)^3\end{aligned} \tag{A3}$$

$$\begin{aligned}J &= (\mathbf{r} \times \mathbf{v}) \left\{ 1 + \frac{1}{2}v^2(1 - 3\eta) + (3 + \eta)\frac{m}{r} + \frac{3}{8}(1 - 7\eta + 13\eta^2)v^4 \right. \\ &\quad \left. + \frac{1}{2}(7 - 10\eta - 9\eta^2)\frac{m}{r}v^2 - \frac{1}{2}\eta(2 + 5\eta)\frac{m}{r}\dot{r}^2 + \frac{1}{4}(14 - 41\eta + 4\eta^2)\left(\frac{m^2}{r}\right) \right\}\end{aligned} \tag{A4}$$

The energy and angular momentum are both measured in units of the reduced rest energy  $\mu = m_2/m$ . For circular orbits  $\ddot{r}_o = \dot{r}_o = 0$  which, from the equations of motion, requires

$$\dot{\phi}_o^2 = \frac{mA_o}{r_o^3}. \tag{A5}$$

This condition reduces to a quadratic in  $\dot{\phi}_o^2$  and we obtain the angular frequency as a function of the radius of the circular orbit for  $\eta > 0$ :

$$\dot{\phi}_o^2[r_o, \eta] = \frac{F - \sqrt{F^2 - H}}{K} \quad (\text{A6})$$

with

$$\begin{aligned} F &= \frac{1}{2}\eta(13 - 4\eta) \left(\frac{m}{r_o}\right)^2 + 1 - (1 + 3\eta) \frac{m}{r_o} \\ H &= 4\eta(3 - 4\eta) \left(\frac{m}{r_o}\right)^2 \left(1 - 2(2 + \eta) \frac{m}{r_o} + \frac{3}{4}(12 + 29\eta) \left(\frac{m}{r_o}\right)^2\right) \\ K &= r_o^2 2\eta(3 - 4\eta) \frac{m}{r_o} . \end{aligned}$$

We show  $\dot{\phi}_o^2(r_o)$  as a function of the circular radius in fig. 16. This gives the complete initial conditions for any circular orbit, stable or unstable.

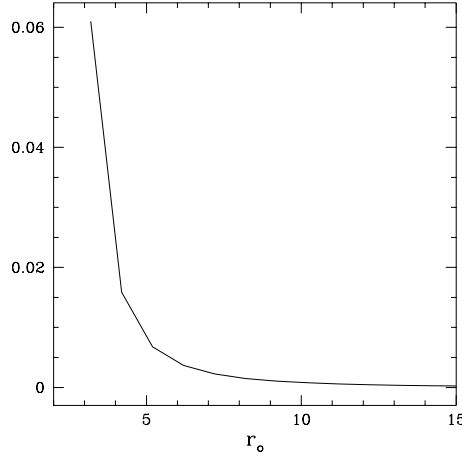


FIG. 16.  $\dot{\phi}_o^2(r_o)$  as a function of the radius of the circular orbit to 2PN order with  $\eta = 1/4$ .

To include the effects of dissipation, the 5/2PN correction needs to be added to  $A$  and  $B$ . They are respectively

$$A_{\frac{5}{2}} = -\frac{8}{5}\eta \frac{m}{r} \dot{r} \left[ 3v^2 + \frac{17}{3} \frac{m}{r} \right] \quad (\text{A7})$$

$$B_{\frac{5}{2}} = \frac{8}{5}\eta \frac{m}{r} \left[ v^2 + 3 \frac{m}{r} \right]. \quad (\text{A8})$$

The instantaneous rate of energy loss to gravitational waves in the far-zone is calculated in Ref. [7] for general orbits to 2PN order. We cite their results here. Defining  $L_{GW} = \left(\frac{dE}{dt}\right)_{\text{far-zone}}^{\text{inst}}$  in units of  $\mu^2$ , they derived

$$L_{GW} = \dot{E}_N + \dot{E}_{1PN} + \dot{E}_{2PN}, \quad (\text{A9})$$

$$\dot{E}_N = \frac{8}{15} \frac{m^2}{r^4} \{ 12v^2 - 11\dot{r}^2 \}, \quad (\text{A10})$$

$$\begin{aligned} \dot{E}_{1PN} &= \frac{8}{15} \frac{m^2}{r^4} \left\{ \frac{1}{28} [(785 - 852\eta)v^4 \right. \\ &\quad - 2(1487 - 1392\eta)v^2\dot{r}^2 \\ &\quad - 160(17 - \eta) \frac{m}{r} v^2 \\ &\quad + 3(687 - 620\eta)\dot{r}^4 + 8(367 - 15\eta) \frac{m}{r} \dot{r}^2 \\ &\quad \left. + 16(1 - 4\eta) \frac{m^2}{r^2} \right\}, \quad (\text{A11}) \end{aligned}$$

$$\begin{aligned}
\dot{E}_{2PN} = & \frac{8}{15} \frac{m^2}{r^4} \left\{ \frac{1}{42} (1692 - 5497\eta + 4430\eta^2) v^6 \right. \\
& - \frac{1}{14} (1719 - 10278\eta + 6292\eta^2) v^4 \dot{r}^2 \\
& - \frac{1}{21} (4446 - 5237\eta + 1393\eta^2) \frac{m}{r} v^4 \\
& + \frac{1}{14} (2018 - 15207\eta + 7572\eta^2) v^2 \dot{r}^4 \\
& + \frac{1}{7} (4987 - 8513\eta + 2165\eta^2) \frac{m}{r} v^2 \dot{r}^2 \\
& + \frac{1}{756} (281473 + 81828\eta + 4368\eta^2) \frac{m^2}{r^2} v^2 \\
& - \frac{1}{42} (2501 - 20234\eta + 8404\eta^2) \dot{r}^6 \\
& - \frac{1}{63} (33510 - 60971\eta + 14290\eta^2) \frac{m}{r} \dot{r}^4 \\
& - \frac{1}{252} (106319 + 9798\eta + 5376\eta^2) \frac{m^2}{r^2} \dot{r}^2 \\
& \left. + \frac{2}{63} (-253 + 1026\eta - 56\eta^2) \frac{m^3}{r^3} \right\} \tag{A12}
\end{aligned}$$

The subscript denotes the order of the term in the PN expansion.

The transverse traceless waveform to  $2PN$  order was also computed in Ref. [7] and we write the instantaneous contribution here for completeness. The Earth is a distance  $D$  from the pair and in a direction  $\hat{N}$ . The vector  $\vec{r}$  is the vector marking the separation of the pair and  $\hat{n}$  the corresponding unit vector. The mass difference is  $\delta m = m_1 - m_2$ . The notation used is  $n_{ij} = n_i n_j$  and, as usual,  $n_{(i} v_{j)} = n_i v_j + n_j v_i$ . The waveform is then

$$\begin{aligned}
h_{km}^{TT} = & \frac{2}{D} P_{ijkm} \left\{ \xi_{ij}^{(0)} + \frac{\delta m}{m} \xi_{ij}^{(0.5)} \right. \\
& \left. + \xi_{ij}^{(1)} + \frac{\delta m}{m} \xi_{ij}^{(1.5)} + \xi_{ij}^{(2)} \right\} \tag{A13}
\end{aligned}$$

with the projection defined as

$$P_{ijkm}(\hat{N}) = (\delta_{ik} - N_i N_k) (\delta_{jm} - N_j N_m) - \frac{1}{2} (\delta_{ij} - N_i N_j) (\delta_{km} - N_k N_m) \tag{A14}$$

and

$$\begin{aligned}
\xi_{ij}^{(0)} &= 2 \left( v_{ij} - \frac{m}{r} n_{ij} \right) \\
\xi_{ij}^{(0.5)} &= \left\{ 3(\mathbf{N} \cdot \mathbf{n}) \frac{m}{r} [2n_{(i} v_{j)} - \dot{r} n_{ij}] + (\mathbf{N} \cdot \mathbf{v}) \left[ \frac{m}{r} n_{ij} - 2v_{ij} \right] \right\} \\
\xi_{ij}^{(1)} &= \frac{1}{3} \left\{ (1 - 3\eta) \left[ (\mathbf{N} \cdot \mathbf{n})^2 \frac{m}{r} \left( (3v^2 - 15\dot{r}^2 + 7\frac{m}{r}) n_{ij} + 30\dot{r} n_{(i} v_{j)} - 14v_{ij} \right) \right. \right. \\
& \quad \left. \left. + (\mathbf{N} \cdot \mathbf{n})(\mathbf{N} \cdot \mathbf{v}) \frac{m}{r} [12\dot{r} n_{ij} - 32n_{(i} v_{j)}] + (\mathbf{N} \cdot \mathbf{v})^2 \left[ 6v_{ij} - 2\frac{m}{r} n_{ij} \right] \right] \right. \\
& \quad \left. + \left[ 3(1 - 3\eta)v^2 - 2(2 - 3\eta)\frac{m}{r} \right] v_{ij} + 4\frac{m}{r} \dot{r} (5 + 3\eta) n_{(i} v_{j)} \right. \\
& \quad \left. + \frac{m}{r} \left[ 3(1 - 3\eta)\dot{r}^2 - (10 + 3\eta)v^2 + 29\frac{m}{r} \right] n_{ij} \right\} \\
\xi_{ij}^{(1.5)} &= \frac{1}{12} (1 - 2\eta) \left\{ (\mathbf{N} \cdot \mathbf{n})^3 \frac{m}{r} \left[ (45v^2 - 105\dot{r}^2 + 90\frac{m}{r}) \dot{r} n_{ij} - 96\dot{r} v_{ij} \right. \right. \\
& \quad \left. \left. - \left( 42v^2 - 210\dot{r}^2 + 88\frac{m}{r} \right) n_{(i} v_{j)} \right] \right. \\
& \quad \left. - (\mathbf{N} \cdot \mathbf{n})^2 (\mathbf{N} \cdot \mathbf{v}) \frac{m}{r} \left[ \left( 27v^2 - 135\dot{r}^2 + 84\frac{m}{r} \right) n_{ij} + 336\dot{r} n_{(i} v_{j)} - 172v_{ij} \right] \right. \\
& \quad \left. - (\mathbf{N} \cdot \mathbf{n})(\mathbf{N} \cdot \mathbf{v})^2 \frac{m}{r} [48\dot{r} n_{ij} - 184n_{(i} v_{j)}] + (\mathbf{N} \cdot \mathbf{v})^3 \left[ 4\frac{m}{r} n_{ij} - 24v_{ij} \right] \right\}
\end{aligned}$$

$$\begin{aligned}
& - \frac{1}{12}(\mathbf{N}\cdot\mathbf{n})\frac{m}{r}\left\{\left[(69-66\eta)v^2-(15-90\eta)\dot{r}^2-(242-24\eta)\frac{m}{r}\right]\dot{r}n_{ij}\right. \\
& - \left[(66-36\eta)v^2+(138+84\eta)\dot{r}^2\right. \\
& - \left.(256-72\eta)\frac{m}{r}\right]n_{(i}v_{j)}+(192+12\eta)\dot{r}v_{ij}\left.\right\} \\
& + \frac{1}{12}(\mathbf{N}\cdot\mathbf{v})\left\{\left[(23-10\eta)v^2-(9-18\eta)\dot{r}^2-(104-12\eta)\frac{m}{r}\right]\frac{m}{r}n_{ij}\right. \\
& - \left.(88+40\eta)\frac{m}{r}\dot{r}n_{(i}v_{j)}-\left[(12-60\eta)v^2-(20-52\eta)\frac{m}{r}\right]v_{ij}\left.\right\} \\
\xi_{ij}^{(2)} = & \frac{1}{120}(1-5\eta+5\eta^2)\left\{240(\mathbf{N}\cdot\mathbf{v})^4v_{ij}-(\mathbf{N}\cdot\mathbf{n})^4\frac{m}{r}\right. \\
& \times \left[\left(90v^4+(318\frac{m}{r}-1260\dot{r}^2)v^2+344\frac{m^2}{r^2}+1890\dot{r}^4-2310\frac{m}{r}\dot{r}^2\right)n_{ij}\right. \\
& + \left.(1620v^2+3000\frac{m}{r}-3780\dot{r}^2)\dot{r}n_{(i}v_{j)}-\left(336v^2-1680\dot{r}^2+668\frac{m}{r}\right)v_{ij}\right] \\
& - (\mathbf{N}\cdot\mathbf{n})^3(\mathbf{N}\cdot\mathbf{v})\frac{m}{r}\left[\left(1440v^2-3360\dot{r}^2+3600\frac{m}{r}\right)\dot{r}n_{ij}\right. \\
& - \left.\left(1608v^2-8040\dot{r}^2+3864\frac{m}{r}\right)n_{(i}v_{j)}-3960\dot{r}v_{ij}\right] \\
& + 120(\mathbf{N}\cdot\mathbf{v})^3(\mathbf{N}\cdot\mathbf{n})\frac{m}{r}(3\dot{r}n_{ij}-20n_{(i}v_{j)}) \\
& + (\mathbf{N}\cdot\mathbf{n})^2(\mathbf{N}\cdot\mathbf{v})^2\frac{m}{r}\left[\left(396v^2-1980\dot{r}^2+1668\frac{m}{r}\right)n_{ij}+6480\dot{r}n_{(i}v_{j)}\right. \\
& - \left.3600v_{ij}\right]\left.\right\}-\frac{1}{30}(\mathbf{N}\cdot\mathbf{v})^2\left\{\left[(87-315\eta+145\eta^2)v^2-(135-465\eta+75\eta^2)\dot{r}^2\right.\right. \\
& - \left.(289-905\eta+115\eta^2)\frac{m}{r}\right]\frac{m}{r}n_{ij} \\
& - (240-660\eta-240\eta^2)\dot{r}n_{(i}v_{j)} \\
& - \left.\left[(30-270\eta+630\eta^2)v^2-60(1-6\eta+10\eta^2)\frac{m}{r}\right]v_{ij}\right\} \\
& + \frac{1}{30}(\mathbf{N}\cdot\mathbf{n})(\mathbf{N}\cdot\mathbf{v})\frac{m}{r}\left\{\left[(270-1140\eta+1170\eta^2)v^2\right.\right. \\
& - \left.(60-450\eta+900\eta^2)\dot{r}^2-(1270-3920\eta+360\eta^2)\frac{m}{r}\right]\dot{r}n_{ij} \\
& - \left[(186-810\eta+1450\eta^2)v^2+(990-2910\eta-930\eta^2)\dot{r}^2\right. \\
& - \left.(1242-4170\eta+1930\eta^2)\frac{m}{r}\right]n_{(i}v_{j)} \\
& + \left[1230-3180\eta-90\eta^2\right]\dot{r}v_{ij}\left.\right\} \\
& + \frac{1}{60}(\mathbf{N}\cdot\mathbf{n})^2\frac{m}{r}\left\{\left[(117-480\eta+540\eta^2)v^4-(630-2850\eta+4050\eta^2)v^2\dot{r}^2\right.\right. \\
& - \left.(125-740\eta+900\eta^2)\frac{m}{r}v^2\right. \\
& + \left.(105-1050\eta+3150\eta^2)\dot{r}^4+(2715-8580\eta+1260\eta^2)\frac{m}{r}\dot{r}^2\right. \\
& - \left.(1048-3120\eta+240\eta^2)\frac{m^2}{r^2}\right]n_{ij} \\
& + \left[(216-1380\eta+4320\eta^2)v^2+(1260-3300\eta-3600\eta^2)\dot{r}^2\right. \\
& - \left.(3952-12860\eta+3660\eta^2)\frac{m}{r}\right]\dot{r}n_{(i}v_{j)} \\
& - \left[(12-180\eta+1160\eta^2)v^2+(1260-3840\eta-780\eta^2)\dot{r}^2\right. \\
& - \left.(664-2360\eta+1700\eta^2)\frac{m}{r}\right]v_{ij}\left.\right\} \\
& - \frac{1}{60}\left\{\left[(66-15\eta-125\eta^2)v^4\right.\right.
\end{aligned}$$

$$\begin{aligned}
& + (90 - 180\eta - 480\eta^2)v^2\dot{r}^2 - (389 + 1030\eta - 110\eta^2)\frac{m}{r}v^2 \\
& + (45 - 225\eta + 225\eta^2)\dot{r}^4 + (915 - 1440\eta + 720\eta^2)\frac{m}{r}\dot{r}^2 \\
& + (1284 + 1090\eta)\frac{m^2}{r^2}\left]\frac{m}{r}n_{ij}\right. \\
& - [(132 + 540\eta - 580\eta^2)v^2 + (300 - 1140\eta + 300\eta^2)\dot{r}^2 \\
& + (856 + 400\eta + 700\eta^2)\frac{m}{r}]\frac{m}{r}\dot{r}n_{(i}v_{j)} \\
& - [(45 - 315\eta + 585\eta^2)v^4 + (354 - 210\eta - 550\eta^2)\frac{m}{r}v^2 \\
& - (270 - 30\eta + 270\eta^2)\frac{m}{r}\dot{r}^2 \\
& \left. - (638 + 1400\eta - 130\eta^2)\frac{m^2}{r^2}\right]v_{ij}\}
\end{aligned}$$

The superscript denotes the order in the PN expansion. A full explanation of the derivation of these terms can be found in the original Reference [7].